Error Estimation and Anisotropic Mesh Refinement for Aerodynamic Flow Simulations

Tobias Leicht and Ralf Hartmann

1 Introduction

We consider steady-state laminar viscous flows governed by the compressible Navier-Stokes equations. In the inviscid limit these degenerate to the compressible Euler equations which are in many cases appropriate to describe flow fields in the presence of shocks.

Our discretization is based on a discontinuous Galerkin (DG) method with the symmetric interior penalty (SIPG) approach for viscous terms[1], see [7, 14] and the references cited therein. The DG approach is a natural extension of the finite volume method predominantly used in aerodynamics to higher order and offers a great flexibility of the underlying meshes concerning both local mesh adaption with hanging nodes and variable order discretizations, combined in hp-algorithms. Being a finite element method a substantial error estimation framework is available.

In the following we will consider constant polynomial degree approximations on quadrilateral and hexahedral meshes with local mesh refinement. Such a refinement is often performed in an isotropic way by splitting all an element's edges and forming new children elements. However, flow phenomena may exhibit a strong directional behavior in boundary layers or interior layers like shocks. Highly stretched elements should be used for an efficient resolution of these features. Starting from a coarse initial mesh, such elements can be obtained by an anisotropic refinement which splits only some of an element's edges.

Considerable work has been devoted to anisotropic refinement for linear finite elements on simplex meshes where the information of an approximated Hessian–based mesh metric field is used within re-meshing algorithms, see [4, 5, 10, 16] for

Tobias Leicht and Ralf Hartmann
DLR(German Aerospace Center), Institute of Aerodynamics and Flow Technology, Center for Computer Applications in Aerospace Science and Engineering, 38108 Braunschweig, Germany, e-mail: tobias.leicht@dlr.de, e-mail: ralf.hartmann@dlr.de

[1] However, results similar to those presented here have also been obtained with the second scheme of Bassi and Rebay [2].

example. Here, the metric field approximates the interpolation error of the solution and is used to determine the local mesh density as well as the local element rotation and stretching in a re-meshing algorithm.

As opposed to a priori interpolation error estimates, a posteriori estimates based on an adjoint problem take into account error transportation and accumulation effects. Using these *goal-oriented* indicators to determine the local mesh density results in meshes which are specifically tailored to the accurate approximation of a target quantity like the aerodynamic lift or drag force. In [18] the directional information of the metric approach has been combined with a scaling based on adjoint-based error indicators, resulting in dual weighted metrics.

Another approach to anisotropy detection in the context of element subdivision is to use several trial refinements and selecting the case which reduces the error most effectively, see [13, 17]. However, such approaches seem unreasonably expensive, especially if they require solutions on globally refined meshes. Solving only local problems and including goal-oriented refinement has been considered in [9].

The purpose of this work is to employ anisotropy indicators which come computationally almost for free, i. e. no auxiliary problems shall be solved for obtaining anisotropic refinement information. Furthermore, these indicators shall be applicable to higher order DG discretizations and they shall be easily combined with different reliable error indicators.

We adopt the partitioned approach of using different indicators for selecting the elements to be refined and for choosing the anisotropic refinement case. In particular, we employ residual-based and adjoint-based indicators for goal-oriented refinement to select a certain fraction of all elements to be refined. In a second step, the discrete solution is analyzed using one of two different anisotropic indicators to decide upon a possibly anisotropic subdivision case. We note, that the presented ideas are only applicable to meshes with tensor-product elements (quadrilaterals in 2D, hexahedra in 3D), whereas other work based on metrics is often only applicable to simplicial meshes.

2 Error Estimation and Error Indicators

Adjoint-based indicators Given a target functional $J(\mathbf{u})$, the error of the discrete solution $\mathbf{u}_h$ compared to the analytical solution $\mathbf{u}$ in terms of the target quantity can be approximated employing a linearized adjoint problem. This corresponds to the well known dual weighted residual (DWR) method by Becker and Rannacher [3], see [14] for an application in the current context. In the DG context the residual and thus this estimate can be decomposed into element-wise contributions which serve as local error indicators.

The total error estimate, i. e. the accumulated local contributions, can be used as a reliable estimate of the discretization error. As this estimates includes the sign of the error it can even be used to improve the computed target quantity value.

Residual-based indicators Assuming that the solution of the adjoint problem is sufficiently smooth, an upper bound of the error in the target quantity can be derived, cf. [7]. The localized form of this estimate serves as residual-based error indicator. As the specific target quantity does not enter the definition of this indicator, it can be used to resolve all flow features but will in general be less efficient for any given target quantity.

3 Anisotropy Indicators

Jump Indicator Assuming that the analytical solution is continuous the presence of discontinuities in the discrete solution indicates local errors. We associate large jumps of the solution over element interfaces with large approximation errors orthogonal to the corresponding face. If the average jump K_i

$$K_i = \frac{\sum_j \left| \int_{f_i^j} (\phi^+ - \phi^-) \, \mathrm{d}x \right|}{\sum_j \int_{f_i^j} 1 \, \mathrm{d}x}, \quad i = 1,2,3, \tag{1}$$

over the two faces f_i^1 and f_i^2 orthogonal to the direction i on the tensor-product reference element is small compared to the maximal value encountered in any direction on the same element we do not refine the element along that direction. Here, $^+$ and $^-$ denote the traces of the function ϕ taken from within the current element and its neighbor, respectively.

If the analytical solution exhibits a discontinuity, e. g. at a shock, close to and almost parallel to a particular face, this indicator will also detect a large jump and refine the element parallel to that face. This is what is required to obtain an improved location of the discontinuity in the numerical solution, thus this behaviour is desirable. The probability that the discontinuity exactly coincides with the face is vanishing for real applications.

Derivative Indicator After a transformation to the reference element to include scaling effects the local interpolation or projection error of a polynomial approximation of degree p to a sufficiently smooth function $\phi \in H^{p+1}$ is determined by the $(p+1)^{\text{th}}$ derivative tensor.

In the general case we compare the projected derivative along the coordinate axes of the reference element and do not refine the element along directions which feature a small derivative compared to other values on that element. For second order methods with $p = 1$ we evaluate the eigenvalues and eigenvectors of the derivative tensor (Hessian) and exclude directions from refinement if they are aligned with the eigenvectors of small eigenvalues.

The underlying smoothness assumption is especially critical for higher order methods and discontinuous solutions at shocks.

Application to Vector Valued Solution Functions Several strategies for extending the presented indicators from scalar valued solution functions ϕ to vector valued solution functions $\mathbf{u}$ have been investigated, see [14] for a comprehensive discussion.

For the jump indicator, we simply replace the jump of the scalar function ϕ in (1) by the jump of the l^2-norm of the vector-valued function $\mathbf{u}$. For the derivative indicator we differentiate between flow regimes: In inviscid cases we simply use the Mach number as a representative scalar variable, whereas in viscous cases the refinement indicator is evaluated separately for each component. We then default to isotropic refinement but select an anisotropic subdivision case if that is suggested by a sufficient number of individual indicators and if there is no contradiction in the predicted direction of anisotropy.

4 Numerical Examples

The basic performance of the proposed indicators will be analyzed using some two-dimensional computations. After that, a three-dimensional example will demonstrate the applicability to flows of increased complexity.

NACA0012 Airfoil Sub-, trans- and supersonic flows around the NACA0012 airfoil according to the flow conditions in Table 1 have been computed on sequences of refined meshes using both adjoint-based and residual-based error indicators as well as isotropic and anisotropic refinement.

Figure 1 plots the error in a selected target functional vs. the number of elements for the different refinement strategies. All reference values have been obtained by fine grid computations. The subsonic case A uses adjoint-based error estimation. Comparing the second order solution of case A1 with the third order solution of case A2 shows the increased accuracy of the method, as a significantly reduced number of elements produces results of the same accuracy in the higher order case. Apart from that the behavior is similar – the jump-based anisotropy indicator significantly reduces the number of elements required for a given accuracy and the derivative-

Table 1: Freestream conditions for NACA0012 test cases

Case	Mach number M	angle of attack α	Reynolds number Re	polynomial degree p	target[a] $J(u)$
A1	0.5	0°	5 000	1	C_{d_p}
A2	0.5	0°	5 000	2	C_{d_p}
B	0.8	1.25°	*inviscid*	1	C_{d_p}
C	1.2	0°	1 000	1	C_{d_f}

[a] C_{d_p} and C_{d_f} denote the pressure and friction part of the drag coefficient $C_d = C_{d_p} + C_{d_f}$, respectively

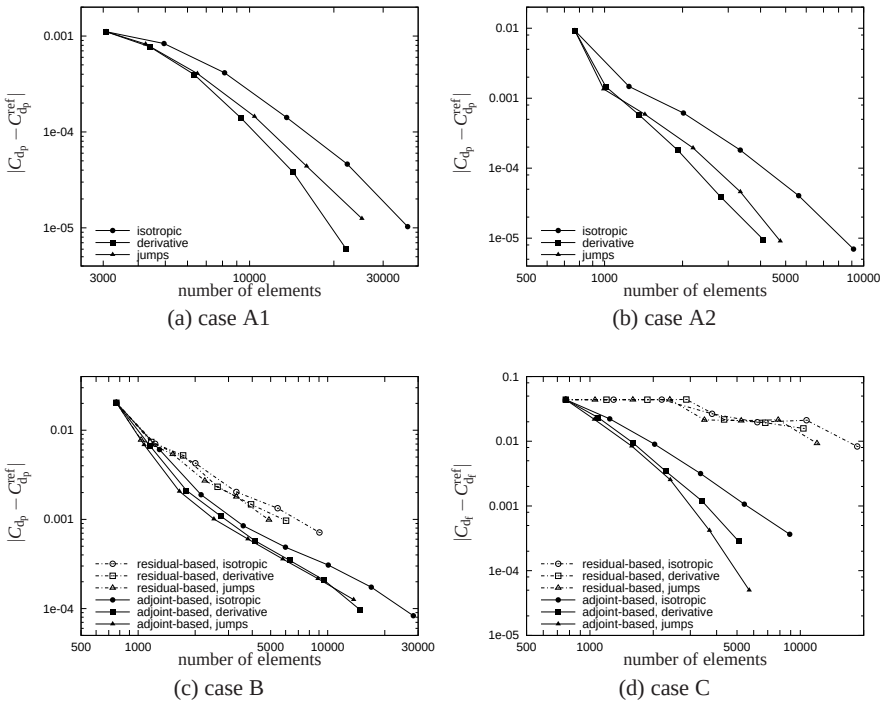

Fig. 1: Convergence of the error under different mesh refinement algorithms for the NACA0012 test cases

based indicator performs even better. As the solution is quite smooth in this subsonic case this can be expected.

Similar results can be seen for the transonic case B. Here the performance of the jump indicator is similar or even superior to the derivative indicator. This is probably due to the reduced smoothness of the solution at the shock which contradicts the assumptions of the derivative indicator. This effect is even stronger in the supersonic case C. In general, the simple jump-based criterion performs remarkably well in all flow regimes.

In transonic cases shocks are usually located in the vicinity of the airfoil and are of great importance for the computed aerodynamic forces. The residual-based indicator resolves these prominent features and thus performs only slightly inferior to the goal-oriented error estimation, see Fig. 1c.

In contrast to that, the supersonic case C features a prominent detached bow shock in front of the airfoil. As the residual-based error estimation initially resolves mainly this feature whereas the boundary layer resolution is improved only later on we notice almost no reduction of the error. Goal-oriented refinement, however, yields significant error reductions already on the first adapted mesh, see Fig. 1d. This motivates the utilization of the adjoint problem in spite of its additional cost.

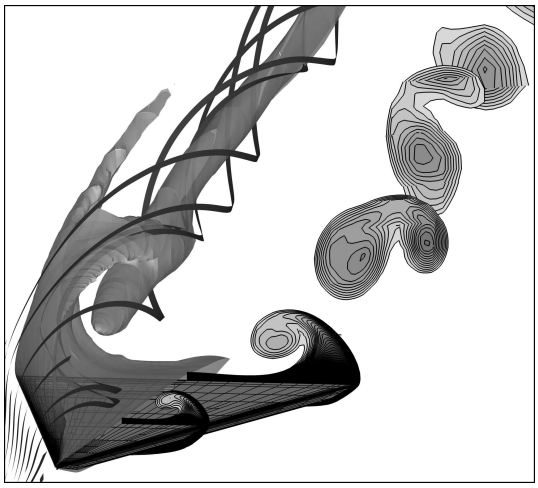

Fig. 2 Solution plot showing streamlines and a Mach number iso-surface over the left half of the delta wing immersed in a laminar flow at high angle of attack as well as Mach number slices over the right half

Laminar Delta Wing As a second more complex example we consider a laminar flow at Mach number $M = 0.3$, Reynolds number $Re = 4\,000$ and an angle of attack $\alpha = 12.5^\circ$ around a delta wing with sharp leading edge and a blunt trailing edge. Figure 2 illustrates the vortex dominated flow characteristics of this test case which has been considered in the EU project ADIGMA [12] and in [8], a similar case was treated earlier in [11].

In the following we consider the error of different approximations of the lift coefficient C_l. Similar results have been obtained for the drag coefficient C_d. We start by computing the lift from the second order flow solution on a sequence of globally refined meshes starting from a very coarse initial 3 264 elemental mesh for the half domain with symmetry boundary conditions. We then consider adaptive local mesh refinement starting from the results on the initial coarse mesh.

Figure 3 plots the error in the lift coefficient vs. the number of elements for various refinement strategies. Compared to global mesh refinement, lift coefficients of a specific accuracy are obtained with less elements for residual-based mesh refinement. We notice that the adjoint-based refinement procedure yields again better results.

Additionally, in case of adjoint-based mesh refinement Fig. 3 illustrates the errors of the enhanced lift coefficients obtained by adding the global error estimate to the computed lift coefficient. Already on the first adapted mesh the enhanced lift coefficient is more accurate than the unmodified values computed on the last adapted meshes.

Finally, we note that anisotropic mesh refinement using the jump indicator performs better than isotropic mesh refinement with an improvement by a factor of almost two on the final mesh in the adjoint-based case. In general, the gain improves for increasing accuracy requirements. Here, the anisotropy indicator works as a general aspect ratio optimizer.

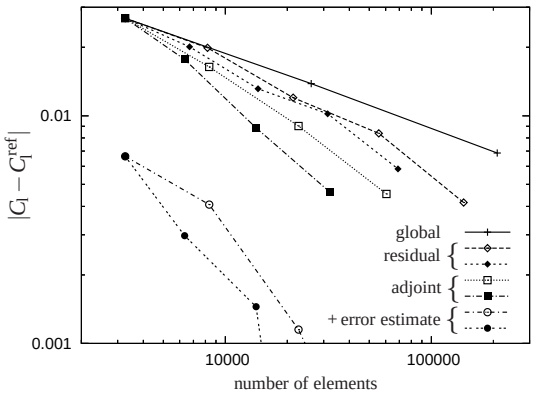

Fig. 3 Laminar delta wing: Error in the computed lift coefficient for sequences of locally refined meshes using different refinement indicators and isotropic (*open symbols*) as well as anisotropic refinement (*filled*)

5 Conclusion and Outlook

The presented anisotropy indicators have been successfully applied to a number of aerodynamic test cases. Especially the very simple jump indicator performs surprisingly well and is thus a good candidate for applications with increased complexity.

So far, only laminar flows with weak boundary layers have been considered. Employing a RANS approach with a suitable turbulence model much thinner and thus stronger boundary layers dominate the flow field. Such cases are of more interest to the aerodynamicist. For theses applications different variables might be of different orders of magnitude, thus the question of how to treat systems of equations efficiently will arise again, perhaps a suitable scaling of the individual components might be necessary.

The presented approach, especially the jump indicator, will also be combined with an *hp*–adaptive algorithm. First experiments show promising results if the number of subdivided elements is not very small compared to the number of elements treated with an increased polynomial order.

Finally, splitting error estimation and anisotropy detection into two distinct indicators is reasonable in many cases but for the purpose of creating nearly optimal meshes for the approximation of a given target functional a combined approach respecting anisotropy in both the primal and dual solution would be ideal. Recently, Richter [15] proposed a unified approach in the context of continuous FEM and a reconstructed dual solution. Extending this approach to our application and to non-tensor-product basis functions will provide an interesting alternative to the proposed algorithm.

Acknowledgements The authors gratefully acknowledge the partial financial support of both the President's Initiative and Networking Fund of the Helmholtz Association of German Research Centres and the European project ADIGMA [12]. All computations have been performed with the flow solver PADGE [6] which employs a modified and extended version of the `deal.II` library [1].

References

1. Bangerth, W., Hartmann, R., Kanschat, G.: deal.II – A general purpose object oriented finite element library. ACM T. Math. Software **33**(4) (2007)
2. Bassi, F., Rebay, S., Mariotti, G., Pedinotti, S., Savini, M.: A high-order accurate discontinuous finite element method for inviscid and viscous turbomachinery flows. In: R. Decuypere, G. Dibelius (eds.) 2nd European Conference on Turbomachinery Fluid Dynamics and Thermodynamics, Antwerpen, Belgium, March 5–7, 1997, pp. 99–108. Technologisch Instituut (1997)
3. Becker, R., Rannacher, R.: An optimal control approach to a posteriori error estimation in finite element methods. Acta Numerica **10**, 1–102 (2001)
4. Formaggia, L., Micheletti, S., Perotto, S.: Anisotropic mesh adaptation in computational fluid dynamics: Application to the advection-diffusion-reaction and the Stokes problems. Appl. Numer. Math. **51**, 511–533 (2004)
5. Frey, P.J., Alauzet, F.: Anisotropic mesh adaptation for CFD computations. Comput. Methods Appl. Mech. Engrg. **194**, 5068–5082 (2005)
6. Hartmann, R., Held, J., Leicht, T., Prill, F.: Discontinuous Galerkin methods for computational aerodynamics - 3D adaptive flow simulation with the DLR PADGE code. submitted to Aerosp. Sci. Technol. (2009)
7. Hartmann, R., Houston, P.: Symmetric interior penalty DG methods for the compressible Navier–Stokes equations II: Goal–oriented a posteriori error estimation. Int. J. Num. Anal. Model. **3**(2), 141–162 (2006)
8. Hartmann, R., Leicht, T.: Error estimation and anisotropic mesh refinement for 3d aerodynamic flow simulations. submitted to J. Comput. Phys. (2009)
9. Houston, P., Georgoulis, E.H., Hall, E.: Adaptivity and a posteriori error estimation for DG methods on anisotropic meshes. In: G. Lube, G. Rapin (eds.) Int. Conference on Boundary and Interior Layers, BAIL2006 (2006)
10. Huang, W.: Metric tensors for anisotropic mesh generation. Journal of Computational Physics **204**, 633–665 (2005)
11. Klaij, C.M., van der Vegt, J.J.W., van der Ven, H.: Space–time discontinuous Galerkin method for the compressible Navier-Stokes equations. J. Comput. Phys. **217**(2), 589–611 (2006)
12. Kroll, N.: ADGIMA – A European project on the development of adaptive higher-order variational methods for aerospace applications. 47th AIAA Aerospace Sciences Meeting (2009). AIAA 2009-176
13. Kurtz, J., Demkowicz, L.: A fully automatic hp-adaptivity for elliptic PDEs in three dimensions. Comput. Methods Appl. Engrg. **196**, 3534–3545 (2007)
14. Leicht, T., Hartmann, R.: Anisotropic mesh refinement for discontinuous Galerkin methods in two-dimensional aerodynamic flow simulations. Int. J. Numer. Meth. Fluids **56**(11), 2111–2138 (2008)
15. Richter, T.: A posteriori error estimation and anisotropy detection with the dual-weighted residual method. Int. J. Numer. Meth. Fluids (2009). DOI 10.1002/fld.2016
16. Sahni, O., Müller, J., Jansen, K.E., Shepard, M.S., Taylor, C.A.: Efficient anisotropic adaptive discretization of the cardiovascular system. Comput. Methods Appl. Mech. Engrg. **195**, 5634–5655 (2006)
17. Sun, S., Wheeler, M.F.: Anisotropic and dynamic mesh adaption for discontinuous Galerkin methods applied to reactive transport. Comput. Methods Appl. Mech Engrg. **195**, 3382–3405 (2006)
18. Venditti, D.A., Darmofal, D.L.: Anisotropic grid adaption for functional outputs: application to two–dimensional viscous flows. J. Comput. Phys. **187**, 22–46 (2003)